ELECTRIC FIELDS AND DOUBLE LAYERS IN PLASMAS

Nagendra Singh, H. Thiemann, and R. W. Schunk
Center for Atmospheric and Space Sciences
Utah State University
Logan, Utah 84322-3400, U.S.A.

ABSTRACT

Various mechanisms for driving double layers in plasmas are briefly described, including applied potential drops, currents, contact potentials, and plasma expansions. Some dynamical features of the double layers are discussed. These features, as seen in simulations, laboratory experiments, and theory, indicate that double layers and the currents through them undergo slow oscillations which are determined by the ion transit time across an effective length of the system in which the double layers form. It is shown that a localized potential dip forms at the low potential end of a double layer, which interrupts the electron current through it according to the Langmuir criterion, whenever the ion flux into the double is disrupted. The generation of electric fields perpendicular to the ambient magnetic field by contact potentials is also discussed. Two different situations have been considered; in one, a low-density hot plasma is sandwiched between high-density cold plasmas, while in the other a high-density current sheet permeates a low-density background plasma. Perpendicular electric fields develop near the contact surfaces. In the case of the current sheet, the creation of parallel electric fields and the formation of double layers are also discussed when the current sheet thickness is varied. Finally, the generation of electric fields (parallel to an ambient magnetic field) and double layers in an expanding plasmas is discussed.

I. INTRODUCTION

Since the early days of double layer (DL) research (e.g., Block, 1972), considerable progress has been made in the understanding of the formation of DL's and their dynamical features. The purpose of this summary is to highlight some of the major findings on the generation of electric fields in collisionless plasmas and on the formation, dynamics, and structure of double layers. We define double layers as electrostatic potential structures that can support localized electric fields in collisionless plasmas. The nomenclature "double layer" is derived from the fact that the electric field is primarily supported by two layers of charges (positive and negative). Such potential structures can form in current carrying plasmas as well as in the absence of a current.

Figure 1 shows a summary of the various mechanisms that can create double layers in a plasma. Broadly speaking, the mechanisms can be categorized as follows:

1. Applied potential drop across a plasma
2. Current through a plasma
3. Contact potentials
4. Plasma expansion.

These mechanisms are not as distinct from each other as it may appear. For example, when a potential drop is applied across a plasma, a current develops (Singh, 1980, 1982; Singh and Schunk, 1982a), or when a current is drawn through a plasma, a potential drop develops (Singh and Schunk, 1982b, 1984a). The characteristics of double layers driven by an applied potential drop and by a current through the plasma have been compared, and they have been shown to be very similar (Singh and Schunk, 1983a).

Contact potentials develop when plasmas with different properties come into contact. The difference in the ion and electron gyroradii plays an important role in creating perpendicular electric fields when the contact surfaces are parallel to the ambient magnetic field. Typically, the scale length of such electric fields is of the order of the ion Larmor radius. The potential structures associated with such electric fields appear as perpendicular or oblique double layers. When the perpendicular electric fields are shorted out at some location away from the source region, it is possible to generate two-dimensional potential structures with electric fields parallel to the ambient magnetic field. Such two-dimensional potential structures are known to play an important role in auroral electrodynamics. It is worth mentioning that the generation of a parallel potential drop by shorting out the perpendicular electric fields away from their source region is, in a sense, equivalent to applying a potential drop. Here, the perpendicular potential drop becomes a parallel potential drop due to the conducting boundary condition.

Current sheets or filaments of a finite thickness in plasmas are examples where the plasma processes driven by both the contact potential and the current take place. Multi-dimensional double layers form in such cases (Singh et al., 1983, 1984, 1985, 1986).

When a high-density plasma expands along an ambient magnetic field into a low-density plasma or into a vacuum, electric fields are set up. Near the expansion front, a double-layer type-charge separation occurs. Thus, currentless double layers form in expanding plasmas (Singh annd Schunk, 1984b).

The purpose of this paper is to present a summary of our studies on the above mechanisms for generating electric fields and double layers. These studies have been performed either with a one-dimensional Vlasov-Poisson solver (Singh, 1980) or with a two-dimensional particle-in-cell (PIC) code (Singh et al., 1983, 1985).

II. APPLIED POTENTIAL DROP

Basically, the process of DL formation is creating a potential drop. Thus, the application of a potential drop across a collisionless plasma may drive a double layer along with a host of other plasma processes (Singh and Schunk, 1982a). There are several laboratory experiments (Coakley and Hershkowitz, 1979; Iizuka et al., 1983, 1985) and numerical simulations (Joyce and Hubbard, 1978; Singh, 1980, 1982; Singh and Thiemann, 1980a,b; Singh and Schunk, 1982a,c, 1983a; Johnson, 1980) in which DL's have been driven by applied potential drops. Some of these experiments and simulations (Singh, 1982; Singh and Schunk, 1982a, 1983a) show remarkable similarities in both the processes leading to the formation of a DL and its dynamics. It is found that these processes are cyclic; the DL formation leads to current interruption, as the DL moves the currents recuperate, leading to the reformation of a new DL. In connection with several space and cosmic plasma phenomena, Alfvén (1982) has invoked the role of exploding double layers, which are cyclic. Thus, it is relevant here to discuss the cyclic behavior of double layers as seen in laboratory experiments and simulations.

Here we illustrate some important plasma processes taking place during recurring DL formation by presenting results from one-dimensional Vlasov simulations (Singh, 1982; Singh and Schunk, 1982a,c, 1983a) in which the dynamics of the plasma of length $0 \leq x \leq d$ is followed by solving the Vlasov and Poisson equations after a potential drop $\Delta\phi_0$ is applied across the plasma. In Figure 2 we present a summary of a simulation in which $d = 100\ \lambda_0$ and $\Delta\phi_0 = 30\ k_B T_0/e$, where λ_0 is the plasma Debye length with T_0 as the electron and ion temperature.

Applying a potential drop across a quasi-neutral plasma is equivalent to applying a uniform electric field E_0 (see the potential profile at $\tilde{t} = 0$ in Figure 2a), whose strength depends on the applied drop $\Delta\phi_0$ and the length of the system; $E_0 \simeq \Delta\phi_0/d$ (Fig. 2a). This field accelerates electrons and ions in opposite directions. However, during very early time ion acceleration is not important, but the electrons are accelerted to the extent that a current is set up in the plasma which may exceed the current at the cathode boundary, $x = 0$ (Fig. 2b). When this happens a positive space charge appears near the cathode ($x = 0$, in Fig. 2) modifying greatly the initial linear potential profile (Fig. 2a). This potential perturbation evolves into an electron hole in the form of a positive potential pulse which propagates in the direction of the initial electric field (Fig. 2a) and it is destroyed when it reaches the anode end. During the phase of the electron hole propagation, counterstreaming electron beams form (Singh, 1982). After this phase the plasma is subject to a strong high frequency turbulence, which modifies the plasma greatly. One important modification is the expulsion of the plasma and creation of plasma cavity. In simulations with very short lengths (Singh, 1980) ($\ell < 100\ \lambda_{do}$), the formation of an extended cavity is not seen. However, as the system length increases, the extended cavity becomes an important feature of the plasma (Singh, 1982; Singh and Schunk, 1982a). Also, the ion flux into the plasma from the anode boundary is totally disrupted; as a matter of fact, an outflux of ions occurs.

The potential step near the cathode evolves into a double layer (Figs. 2a, c, and d) self-consistently modifying the electron and ion velocity distribution functions. Soon after its formation, the DL develops a potential dip (potential profiles marked with "A" in Fig. 2e) at its low potential end which interrupts the electron current (bottom panel in Fig. 2e) and it moves toward the anode (compare potential profiles "A" and "B" in Fig. 2e). The moving double layer sits on an expanding plasma density front moving approximately at the ion-acoustic speed (Singh and Schunk, 1982b). The expanding plasma and the ion acceleration by the double layer produce counterstreaming ion beams near the low potential end of the DL (Singh and Schunk, 1982a). In the frame of reference of the moving double layer, the electron and ion current continuity conditions are maintained (Singh and Schunk, 1982a).

As the double layer moves, the ion flux (current) at the anode reverses from outflux to influx (Fig. 2e). As the ion current through the DL recuperates, so does the electron current approximately satisfying the Langmuir condition (Singh and Schunk, 1982c). In the presence of the ion beam and the electron current on the low potential side, any positive potential perturbation near the cathode triggers the reformation of the double layer and the above plasma processes repeat in a cyclic fashion (Fig. 2e). The time constant of this cyclic process is the ion transit time (τ_i) across the system or equivalently the transit time of the double layer across the system. The above cyclic phenomenon of DL formation is summarized in Figure 3. The cyclic reformation of double layers has been seen in simulations with applied potential drops reported by other authors (Joyce and Hubbard, 1978; Borovsky and Joyce, 1983).

Some of the cyclic processes seen in the simulations have also been seen in laboratory experiments (Iizuka et al., 1983, 1985). These experiments were carried out in a Q machine with both single- and double-ended operations. In the single-ended operation only the cathode plasma source was operative. On the other hand, in the double-ended operation both the cathode and anode plasma sources were operative. Iizuka et al. (1983) clearly show that in both types of operations, cyclic behaviors were seen, but there were some differences between them as discussed below. With the single-ended operation, the double layer formed near the cathode and subsequently moved toward the anode and disappeared there, and with the applied potential drop persisting, a new double layer formed near the cathode and moved away from it. Thus, the double layer appears to show a forward (toward anode) and backward motion. However, the backward motion (toward cathode) was found to be so fast that the details of the plasma processes during this phase could not be resolved in the experiments. From our simulations we find that the time scale of the rise in the potential at the low potential end of the double layer, which eventually leads to the formation of a new double layer (Fig. 2f), is roughly $\tau_r < 100\ \omega_{po}^{-1}$. For the plasma densities ($\sim 10^8\ cm^{-3}$) in the experiment, $\tau_r \simeq 0.1\ \mu s$ which is much smaller than the temporal resolution of about 1 μs in the experiments.

C-3

In double-ended operations, Iizuka et al. did not see the motion of the whole double layer; instead, a back and forth motion of the low potential end of the double layer was seen. In agreement with the single-ended operation, the backward motion was found to be so fast that it could not be resolved in the experiment while the forward motion was slow. These motions were correlated with the oscillation in the current at a frequency determined by the transit time of the low potential end during its forward motion. Such features of double layers seen in the Q machine with the double-ended operations are common in simulations with very short system lengths (Singh, 1980; Singh and Thiemann, 1980a).

The cyclic behavior seen in the simulations and laboratory experiments driven by applied potential drops has also been seen in simulations (Singh and Schunk, 1982b, 1983a, 1984a) and experiments (Leung et al., 1980) in which double layers were driven by current injections.

It is important to assert here that the cyclic behavior seen in the simulations and experiments do not appear to be an artifact of the boundary conditions. The primary cause of the cyclic behavior appears to be the fundamentally different time scales associated with the electron and ion dynamics. The plasma processes which lead to the double layer formation interrupt the ion flux into the double layer. Due to the lack of the ion flux, the double layer moves and also the current through it disrupts according to the Langmuir condition (Singh and Schunk, 1982c). When the ion flux recuperates slowly, so does the electron current. Some plasma fluctuations on the low potential side, after the current recovery, start the process of double layer reformation. In the simulations, the fluctuations are found to be growing electron holes, which appear to be caused by the rarefaction instability (Carlqvist, 1972; Block, 1972; Singh, 1982).

The cyclic oscillations discussed above appear to be in accord with the theoretical work of Silevitch (1981), who showed that in an unbounded plasma, strong double layers have a negative dynamic resistance. Thus, only when the system (circuit), of which the double layer is a part, is sufficiently "lossy," it is possible to create a steady double layer. Otherwise, the double layer oscillates with a frequency determined by an effective ion transit time (Silevitch, 1981).

It is worthwhile to mention that Smith (this proceedings) draws quite different conclusions from those drawn here regarding the cyclic behavior of double layers as seen in simulations and experiments. His discussion on the experimental results with the double-ended operation of the Q machine and the comparison of the results from experiments (Iizuka et al., 1983) with those from simulations (Singh and Schunk, 1982a,c) are misleading.

The cyclic behaviors of the double layer and the current through it, as discussed here, may be relevant to some space and cosmic plasma phenomena such as magnetic storms, solar flashes, and solar flares, which are found to be repetitive (Alfvén, 1982). It has been suggested that these phenomena may be caused by exploding double layers (Alfvén, 1982) which are caused by the inductive effects in the current systems in the plasma. When the double layer forms, the current interrupts. The decreasing current may induce large voltages which add to the double layers. The repetitive feature appears because of the subsequent current recovery. The time scale (τ_c) of such recovery may be determined by the circuit properties. If $\tau_c << \tau_i$, the current recovery through a DL is dictated by the time scale of the ion transit time. Otherwise ($\tau_c >> \tau_i$), the repetition time is determined by τ_c. For a given space or cosmic situation it is possible to make rough estimates of τ_i (Singh and Schunk, 1982c), but it is difficult to estimate τ_c because of the distributed nature of the circuit properties associated with the currents.

As an illustrative example, let us consider the auroral circuit. If we assume that circuit length parallel to the geomagnetic field is $\ell_{\|} \simeq R_e$, the Earth radius, the transit time of an ionospheric hydrogen ion with thermal energy $\sim$ 1 eV is $\tau_i \simeq 500$ s. For an auroral circuit, Alfvén (1982) estimated the inductance $L \simeq 30$ H. Assuming the resistance in the circuit to be $R \simeq 0.1$ ohm, $\tau_c = 300$ s. However, we note that these numbers are highly tentative. It is not even certain that for the auroral double layer, which exists in extended auroral cavity, the transit times across or along the field lines are relevant (Singh and Schunk, 1982c).

III. CURRENT INJECTION

The above cyclic process leading to double layer reformation has been seen in laboratory experiments (Leung et al., 1980) and simulations (Singh and Schunk, 1982b, 1984a) when electron current is injected into the plasma. However, there are some important differences in the formation processes of the double layers driven by current injection or applied potential drop. In the former case when the electron drift velocity is sufficiently large the Buneman instability leads to the double layer formation. In the early stage of the Buneman mode relatively small scale waves grow (see early time ($\tilde{t} < 1920$) plots Fig. 4a). During the nonlinear stage of the instability the small scale oscillations transform into long wavelength ones ($1920 < \tilde{t} < 2000$; Fig. 4a). Further evolution of the waves leads to formation of solitary pulses ($t \gtrsim 2000$; Fig. 4a). The double layers evolve from these pulses by self-consistent modification of the electron and ion distributions.

IV. DOUBLE LAYER STRUCTURE

During their temporal evolution, double layers undergo considerable modification in their potential distribution which critically depends on the current through the double layers. In this section we illustrate this through an example in which the plasma was driven by a current as discussed in Section III. However, it is important to note that the features discussed here are quite general. Figure 4b shows the temporal evolution of the double layer potential profile after the initial evolution shown in Figure 4a. The corresponding temporal evolutions of the average electron drift ($\tilde{V}_{de}$), electron thermal velocity ($\tilde{V}_{te}$), electron current ($\tilde{J}_e$), and electron temperature ($\tilde{T}_e$), all quantities being on the low potential side ($\tilde{x} = 50$), are given in Figure 4c. At early time ($\tilde{t} < 2340$), when the current density is large ($|\tilde{J}_e| > 1.5$), multiple double layer formations with typical double layer dimension $\ell_{DL} \simeq 20\,\lambda_{do}$ are seen. On the other hand, when the current interrupts suddenly at $\tilde{t} = 2345$, the double layer develops a localized potential dip at its low potential side. At such times $\tilde{V}_{de} < \tilde{V}_{te}$. The sudden electron current interruption is seen to be accompanied by a disruption in the ion influx caused by the strong solitary pulse at $\tilde{t} = 2345$. Figure 4d shows the structure of the double layers with a dip by plotting the electron and ion density profiles along with the potential profile. Considering the charge separation (Fig. 4d) we note that the potential distribution is a triple layer. However, its predominant nature, as determined by the large electric field, is still of double layer type. The dip plays the role of a current interruptor to adjust the electron current in accordance with the ion influx so that the Langmuir condition is met.

The formation of a dip at the low potential end of a weak ion-acoustic (IA) double layer has been known since its first observation in numerical simulations (Sato and Okuda, 1981). The interesting fact to note is that the formation of an IA double layer itself depends on such dips (Hasegawa and Sato, 1982). On the other hand, we have shown here that in the case of an already existing double, whether weak or strong (Singh et al., 1985), the current interruptions lead to the formation of such dips.

V. DOUBLE LAYER SCALE LENGTHS

Several simulations and laboratory experiments have indicated that for strong double layers the scale length L is given by (Joyce and Hubbard, 1978, Singh, 1980),

$$L \simeq 6\,(e\Delta\phi_{DL}/k_B T_o)^{1/2} \quad . \tag{1}$$

This scaling has been empirically derived from simulations based on applied potential drops. We find that when double layers evolve from waves or wavelets, such as the electron holes (Fig. 4b), the double layer scale length is typically of the order of the scale length of the perturbations from which the DL evolves.

VI. CONTACT BETWEEN DIFFERENT PLASMAS

The existence of contact potentials (electric fields) near the contact surface between two materials having different electrical properties is a well-known phenomenon. In plasmas, the existence of such potentials has been investigated in connection with plasma confinement (e.g., see Sestero, 1964). In space plasmas, the studies related to the structure of the magnetopause indicate that this is a region where contact potentials can develop (e.g., see Whipple et al., 1984 and references therein). Several years ago, Hultqvist (1971) suggested that the contact between the hot plasma in the plasma sheet and the cold ionospheric plasma may create magnetic field-aligned (parallel) electric fields which could account for the observed precipitating energetic ions along the auroral field lines. More recently, Barakat and Schunk (1984) suggested that the contact between the cold polar wind electrons and the hot polar rain electrons may create parallel electric fields.

It is now clear that electric fields perpendicular to the geomagnetic field are an important feature of the auroral plasma. However, the mechanisms for creating such fields have not been well established. It is possible that they are supported by discontinuities in the plasma properties (such as particle temperatures and densities) across magnetic field lines. Such discontinuities, in which the normals to the plane of the discontinuities are perpendicular to the magnetic field lines, are known as tangential discontinuities.

Even though the existence of perpendicular electric fields in the auroral plasma is well established, the nature of the plasma discontinuities (associated with the fields), if they exist, remains virtually unexplored. Recently, however, Evans et al. (1986) have presented observational evidence that tangential discontinuities do occur in association with discrete auroral arcs. They also conducted one-dimensional steady-state calculations on the generation of perpendicular electric fields through the contact of a high-density hot plasma with a low-density relatively cold plasma. They obtained electric fields having scale lengths of both the electron and ion Larmor radii. This is expected because in their model the electrons were not highly magnetized; they used $\Omega_e/\omega_{pe} < 1/3$, where Ω_e and ω_{pe} are the electron-cyclotron and electron-plasma frequencies, respectively. However, in the auroral plasma, where the large perpendicular electric fields have been observed, typically $\Omega_e >> \omega_{pe}$, implying highly magnetized electrons.

Motivated by the observations of large perpendicular electric fields in the auroral plasma, we have pursued two different approaches for creating perpendicular fields by contact potentials as follows:

1. When a low-density containing sufficiently hot ions is sandwiched by high-density cold plasmas, it is possible to generate electric fields having strengths comparable to those observed in the auroral plasma. In such a situation the electric fields occur near the edges of a cavity in the plasma density as it is sometimes the case in the auroral plasma (Mozer and Temerin, 1983).

2. Upward field-aligned currents are a well-known phenomenon in the auroral plasma. These currents can occur in the form of thin sheets or filaments. We study such a situation by driving currents through a background plasma. The currents flow in sheets of finite thicknesses. The contact between the plasmas inside and outside the sheet produces perpendicular electric fields.

By means of numerical simulations, we have studied the above mechanisms for the generation of perpendicular electric fields. We briefly summarize our studies in the following two subsections.

A. Perpendicular Electric Fields Near the Contact Surface Between Hot and Cold Plasmas

Figure 5 shows the geometrical scheme of our simulations. Using a standard particle-in-cell code (Morse, 1970), we simulate a two-dimensional plasma of size $L_x \times L_y$. The magnetic field **B** is along the y-axis. It is assumed that all field quantities and plasma properties are invariant along the z-axis. In order to study the generation of the perpendicular electric fields, the plasma is stratified along the x-axis. The simulation plasma is divided into regions I, II, and III, which are initially (time $t = 0$) filled with plasmas with different properties. For this study, the plasmas are as follows. In region I, $n_{i1} = n_{e1} = n_o$, where n denotes density and subscripts e, i, and 1 refer to electrons, ions, and region I, respectively; the electron temperature $T_{e1} = T_0$ and the ion temperature T_{i1} is varied in the different simulations. In regions II and III, the plasma properties are the same: $n_{i2} = n_{e2} = n_{i3} = n_{e3}$ and $T_{i2} = T_{e2} = T_{i3} = T_{e3} = T_c$. The temporal evolution of the plasmas for $t > 0$ is followed by calculating the particle dynamics with the self-consistent electric fields.

In our simulations we use the electrostatic approximation. Thus, the electric fields are calculated by solving the Poissson equation with the following boundary conditions: $\phi(x = -L_x/2,y) = \phi(x = L_x/2,y) = 0$. Note that these are the Dirichlet conditions on the electric potential ϕ. Along y we use a periodic boundary condition, implying $\phi(x,y = 0) = \phi(x,y = L_y)$. The electric field **E** is obtained from $\mathbf{E} = -\nabla\phi$.

In the simulations described here, we ignore the magnetic fields generated by the plasma currents, which flow near the plasma interfaces. Thus, the ambient magnetic field remains unperturbed. Such an assumption appears justified at altitudes up to a few Earth radii, where the geomagnetic field is strong and the particle pressures are much smaller than the magnetic pressure.

We use the following definitions and normalizations: density $\tilde{n} = n/n_o$; temperture $\tilde{T} = T/T_o$, where n_o and T_o are the initial (time $t = 0$) density and electron temperature in region I; distance $\tilde{x} = x/\lambda_{do}$; velocity $\tilde{V} = V/V_{to}$; time $\tilde{t} = t\omega_{po}$; electric potential $\tilde{\phi} = e\phi/k_BT_o$; electric field $\tilde{E} = E/E_o$; current $\tilde{J} = J/(n_oeV_{to})$, where $V_{to} = (k_BT_o/m_e)^{1/2}$, $\omega_{po} = n_oe^2/m_e\varepsilon_o$, $\lambda_{do} = V_{to}/\omega_{po}$, $E_o = k_BT_o/e\lambda_{do}$, k_B is Boltzmann's constant, and m_e is the electron mass. In the simulations we use an artificial ion mass, $m_i = 64m_e$.

The results described in the following sections are taken from simulations in which $L_x \times L_y = 64 \times 64\,\lambda_{do}^2$, $d = 32\,\lambda_{do}$, $\Omega_e/\omega_{po} = 4$, where Ω_e is the electron cyclotron frequency, and where the number of electrons and ions per cell of dimension λ_{do}^2 was 4 in region I and 16 in regions II and III.

When the plasma properties change along a direction perpendicular to the magnetic field, as in Figure 5, the ions play a crucial role in creating the contact potential near the interfaces between the different plasmas. As long as the ion temperature $T_i > (m_e/m_i)^{1/2}T_e$, where T_e is the electron temperature, the ion Larmor radius $\rho_i > \rho_e$, the electron Larmor radius. Thus, ions from the neighboring plasmas penetrate the interface more effectively than do the electrons. Thus, depending on the relative densities and the ion temperatures in the neighboring plasmas, a contact potential may develop.

There are numerous possibilities for choosing the relative densities and temperatures in region I to III of Figure 5. In this study, we were primarily motivated by the observations of perpendicular electric fields near the edges of density cavities (Mozer and Temerin, 1983). Thus, we chose $\tilde{n}_2 = \tilde{n}_3 = 4$ and $\tilde{n}_1 = 1$. We assumed that the dense plasmas in regions II and III were cold and that they had the same temperature $T_c < T_o$. On the other hand, the electrons and ions in region I were assumed to be warmer than those in the other two regions. We present results on the effect of the variation of the warm ion temperature on the perpendicular electric fields that developed near the contact surfaces.

Figure 6 shows the distributions of the electric potential, the perpendicular electric field, and the plasma density as functions of $\tilde{x}$ at $\tilde{t} = 100$ for $T_c = 0.2\,T_o$, and $T_{i1} = 20\,T_o$. Recall that $T_{e1} = T_o$. Thus, in the low-density plasma of region I, the ions are hotter than the cold ions in regions II and III by a factor of 100. We note that the average Larmor radius of the hot ions $\rho_H \simeq 9\,\lambda_{do}$. The quantities shown in Figure 2 are time-averaged over a time interval of $\Delta\tilde{t} = 50$ centered at $\tilde{t} = 100$.

Figure 6a shows that a negative potential valley develops in region I ($|\tilde{x}| < 16$). The large perpendicular electric fields develop near the contact surfaces, where sharp gradients occur in the density (Fig. 6b). The maximum magnitude of the electric fields is approximately $\tilde{E}_\perp \simeq 0.6$ and the scale length of the electric field near each interface is about $\rho_H \simeq 9\,\lambda_{do}$.

We find that such large electric fields develop only when the ions in region I are sufficiently warm. In order to show this we carried out simulations by varying the hot ion temperature T_{i1}. For $T_{i1} = T_o$, we did not find any enhancement in $E_\perp$ near the interfaces. As the ion temperature T_{i_1} was increased, bipolar electric fields developed near the interfaces; for $T_{i1}/T_o = 5$, $E_{\perp max} \sim 0.2$. It was found that for $T_{i1}/T_o > 10$, $E_{\perp max}$ does not increase indefinitely, but for the parameters used in the simulation it is limited to about $\tilde{E}_{\perp max} \lesssim 0.6$.

A noteworthy feature was found that is that the electric fields maximize just inside the low-density plasma and not at the interface (Fig. 6). This happens because the gyrating cold ions in the high-density plasmas of regions II and III partially neutralize the space charges created by the hot gyrating ions near the interfaces. In Figure 6 the magnitude of the hot ion Larmor radius ρ_H is indicated. The electric fields at the interfaces have scale lengths of the order of the Larmor radius.

The temporal evolution of the potential drop $\Delta\phi = \phi(x = 0)$ in the simulations show that at early times ($\tilde{t} < 20$) the potential drop grows and afterward undergoes a slow oscillation, with time-averaged values depending on the hot ion temperature T_{i1}. It is worth mentioning that the time constant (τ_{cont}) for the development of the contact potential ($\Delta\phi$) is approximately given by

$$\tau_{cont} \sim 20\,\omega_{po}^{-1} \sim \Omega_i^{-1} \quad , \tag{2}$$

where Ω_i is the ion-cyclotron frequency ($\Omega_i \simeq eB/m_i$). By varying Ω_e/ω_{po}, we found that the above scaling of τ_{cont} with Ω_i is generally valid. Thus, the contact potential sets up with a time constant that is associated with the ion cyclotron motion.

The slow oscillations occur at the ion-plasma frequencies of the plasmas in regions I and II. Comparing the relative amplitudes of $E_\perp$ and $E_\parallel$ associated with the oscillations, we find that $E_\perp >> E_\parallel$. Thus, these oscillations are not of the ion-acoustic type, but are associated with the lower hybrid frequencies in regions I to II.

It is important to note that the geometry of our simulations does not allow the excitation of drift modes propagating in the direction of the diamagnetic currents near the interfaces at $x = \pm d/2$. These currents flow along the z-axis. We have assumed in our simulations that all physical quantities are invariant with respect to z. Thus, no wave modes are allowed to propagate in this direction.

The contact potential develops because the hot ions in region I, while gyrating, penetrate into the neighboring plasmas of regions II and III. In order to show this, the ion velocity distribution function (F) is plotted in Figure 7 as a function of the x-component of the ion energy, $W_x = 1/2\,m_iV_x^2 = 32\,\tilde{V}_x^2 k_B T_o$, at several locations for the simulation with $T_{i1}/T_o = 15$. The distribution at $x = 0$ (center of region I) clearly matches the initial Maxwellian distribution with a temperature $\tilde{T}_{i1} = 15$, as shown by the asymptote marked with this temperature. On the other

hand, at $\tilde{x} = 32$ (near the end of region III) the ion population is cold. At $\tilde{x} = 24$, we see that the hot and cold ions have mixed together. The average ion Larmor radius for the hot ions in region I for $\tilde{T}_{i\parallel} = 15$ is $\tilde{\rho}_H \simeq 8$. Thus, we expect the penetration of a large number of hot ions from region I($|\tilde{x}| < 16$) into region III up to a distance of about $\tilde{x} \simeq 24$. This is verified by the distribution function at $\tilde{x} = 24$. The distribution at $\tilde{x} = 16$ is near the initial interface, where we see that compared to the numbers of ions in the cold and hot populations at $\tilde{x} = 24$, the number of ions in the cold population has decreased, while that in the hot population has increased.

We summarize this section by noting that when a low-density plasma containing hot ions comes into contact with a high-density cold plasma with the contact surface being parallel to the magnetic field, it is possible to create perpendicular electric fields. The time constant for creating such fields is roughly Ω_i^{-1} and the scale length is approximately ρ_H, the Larmor radius of the hot ions.

The above results indicate that when the hot ion temperature $T_{i\parallel} > 10\, T_o$, a rough estimate of the strength of the perpendicular electric field is

$$E_\perp \sim 0.5\, E_o \quad , \tag{3}$$

where the normalizing electric field E_o critically depends on n_o and T_o. When n_o varies from 1 to 10 cm^{-3} and T_o varies from 1 to 100 eV, the strength of $E_\perp$ ranges from several tens to several hundreds of mV/m. Satellite observations indicate that the electric fields associated with electrostatic shocks (Mozer et al., 1980) have a similar strength. For example, if we assume that the hot plasma in region I is of plasma sheet origin and the electron temperature T_o = 100 eV, then it is possible to create perpendicular electric fields of several hundreds of mV/m if the hot ion temperature $T_{i\parallel} > 1$ keV, which is common in the plasma sheet. For $T_o = 100$ eV, the cold plasma temperature assumed in our simulations is $T_c = 20$ eV. We find that when T_c is reduced below $0.2\, T_o$, as assumed here, this does not significantly affect the electric fields. Thus, the cold plasma may originate in the ionosphere.

However, the question of how the stratification of the plasma assumed in our simulations (Fig. 5) is created in space plasmas still needs to be answered. It now appears that plasma blobs and clouds are created in the magnetotail region. When these blobs of plasma move closer to the Earth where a colder plasma exists, the stratification of the plasma assumed in our simulations may be created.

In this section we were mainly concerned with the generation of perpendicular electric fields. In the near future we will study the creation of parallel electric fields, the formation of double layers, the parallel acceleration of electrons and ions, and the generation of parallel currents that occurs when the perpendicular electric fields generated by contact potentials are shorted out by a conducting boundary. Such studies will complement our previous studies on current sheets as summarized in the next section.

B. Double Layer Structures Associated with Current Filaments or Sheets

There are evidences that the current systems in space and cosmic plasmas are filamented (e.g., see Alfvén, 1982 and references therein). Thus, there is a need to study double layer structure in filamentary currents. The available temporal and spatial resolutions for the plasma measurements in the auroral region indicate that the field-aligned currents are highly structured in the form of current sheets with north-south thicknesses of a few kilometers (Dubinin et al., 1985). Probably even thinner sheets exist but they have not been resolved.

Here we briefly summarize our recent efforts on simulations of double layers driven by current sheets (Singh et al., 1983, 1984, 1985; Thiemann et al., 1984). Figure 8 shows our simulation scheme. A two-dimensional

plasma of size $L_x \times L_y$ is driven by a magnetic field-aligned current sheet having a current density J_o. Initially the simulation region is filled with a plasma of density n_o and temperature T_o. At later times, particles are injected both at the top and lower boundaries. Electrons and ions injected at the top boundaries have temperature T_o and T_{iu} (T_H) while those at the lower boundary $T_{i\ell}$ and $T_{e\ell}$. Various simulations were performed by varying these temperatures using a standard particle-in-cell (PIC) code. The electron current is set up in the sheet by injecting electrons at the top of the current sheet at rates to produce desired current (flux) densities. These electrons were also given a downward drift V_{de}. Overall, charge neutrality of the simulation plasma was maintained by counting the number of electrons and ions and injecting an appropriate number of the deficient particles at the lower boundary. The electrostatic boundary conditions are as follows; the plane $y = 0$ is assumed to be conducting, $\phi(x,y = 0) = 0$; at the top boundary we set $E_y(x,y = L_y) = 0$ and a periodic boundary condition was used in x.

We use the following definitions: λ_{do} is the Debye length based on the temperature T_o and on the initial density of $n_o = 4$ particles per cell, Ω_e is the electron-cyclotron frequency and $\omega_{po}^2 = n_o e^2/m\varepsilon_o$, where ε_o is the permittivity of free space and m is the electron mass. The ion-electron mass ratio was chosen to be $M/m = 64$. In the analysis that follows, we use the following normalizations: distance $\tilde{y} = y/\lambda_{do}$, time $\tilde{t} = t\omega_{po}$, velocity $\tilde{V} = V/V_{to}$, potential $\tilde{\phi} = e\phi/k_B T_o$, electric field $\tilde{E} = E/E_o$, $E_o = (k_B T_o/e\lambda_{do})$, and current density $\tilde{J} = J/(en_o V_{to})$, where $V_{to} = (k_B T_o/m_e)^{1/2}$. The numerical technique used here has been previously described in much greater detail by Singh et al. (1985).

Figure 9 shows an example of the potential structure as seen in a simulation in which $\ell = 12\,\lambda_{do}$, $\rho_H = 9\,\lambda_{do}$, $\rho_{i\ell} = 4\,\lambda_{do}$, $\Omega_e/\omega_{po} = 2$, $\tilde{J}_o = 1.25$, $T_H/T_o = 5$, $T_{e\ell} = T_{i\ell} = T_o$, and $L_x \times L_y = 64 \times 128\,\lambda_{do}^2$, where ρ_H and $\rho_{i\ell}$ are the Larmor radii of the ions injected at the top and bottom of the simulation plasma, respectively. The potential structure is illustrated by plotting (a) equipotential surfaces, (b) contours of constant $E_\perp$, the component of the electric field perpendicular to the magnetic field, and (c) contours of constant $E_\parallel$, in x – y plane. The current sheet edges are indicated by the arrows at the bottom of each panel. The solid and broken line contours show positive and negative values of the quantities. A V-shaped potential structure is evident from panel (a); a negative potential valley develops in the upper portion of the current sheet. Panel (b) shows the occurrence of a large bipolar perpendicular electric field near the edges of the current sheet at the top of the simulation plasma. The perpendicular electric fields develop due to the contact between the high-density plasma inside the sheet with a low-density plasma around it (Kan and Akasofu, 1979; Wagner et al., 1980; Singh et al., 1983). The hot ion Larmor radius determines the perpendicular scale length of the electric fields. The V-shaped potential structure develops when the perpendicular electric fields originating near the top of the simulation plasma are shorted out by the conducting surface at y = 0, thus, creating a parallel potential drop.

Panel (c) of Figure 10 shows the localized parallel upward electric fields as indicated by the "H" inside the current sheet. These parallel fields are of double layer type. There are three double layers stacked on top of each other inside the current sheet. The existence of these double layers can also be inferred from the equipotential surfaces in Figure 9a. Typically the maximum electric field strength in the double layers is about $\tilde{E} = 0.25$. The scale length of the double layers along the magnetic field is found to be about $10\,\lambda_{do}$ while they fill the entire width of the current sheet.

The double layers shown here are not dc, but they undergo considerable temporal variations at time scales ranging from electron to ion-plasma periods. Figure 10a shows the temporal variation in the double layer potential profile after averaging out the fast electron oscillations. Note the considerable changes in the potential profile and as well as in the magnitude of the net potential drop across the double layer. The temporal variations in $E_\parallel$ and $E_\perp$ at the point (0, 100) in the region of double layer formation, are shown in Figure 10b. Even at the times when $E_\parallel$ has a dc component, there are considerable fluctuations in both $E_\parallel$ and $E_\perp$. These fluctuations appear to have frequencies ranging from below the ion-cyclotron frequency to above the lower hybrid frequency. In addition, $E_\parallel$ is found to have high frequency oscillations up to electron-plasma frequency and its harmonic which are averaged out in Figure 10b. The high frequency oscillations are not seen in $E_\perp$.

In a narrow current sheet, as discusssed above in context of Figures 9 and 10, it is difficult to distinguish clearly between the double layers inside the current sheet and the large perpendicular electric fields occurring near the edges of the sheet. On the other hand, in wide sheets ($\ell >> \rho_H$), the double layers inside the current sheets are well separated from the large $E_\perp$ occurring near the edges. Figure 11 shows an example of a potential structure associated with a current sheet of thickness $\ell = 32\,\lambda_{do}$, and $\ell/\rho_H \simeq 10$. Panel (a) shows the equipotential surfaces in the x – y plane, panel (b) shows the perpendicular distributions of $E_\perp(x)$ and $\phi(x)$ at $y = 120\,\lambda_{do}$, and panel (c) shows the perpendicular distribution of $J_\parallel(x)$ at $y = 120\,\lambda_{do}$. In this simulation maximum possible value of the upward current in the sheet is $J_o \simeq 0.6\,n_o e V_{to}$. Note that only weak potentials ($\sim k_B T_o/e$) develop inside the sheet, and the regions exterior to the sheet near the top (panel a) are highly positive. The perpendicular potential profile in the sheet is quite flat (panel b). Thus, $E_\perp$ is mostly confined near the edges. In the region of large $E_\perp$ near the edges we find that $E_\perp >> E_\parallel$, which is an important feature of the electrostatic shocks observed in the auroral plasma (Mozer et al., 1980). On the other hand, inside a wide sheet where double layers from $E_\perp \sim E_\parallel$ and both $E_\perp$ and $E_\parallel$ are considerably smaller than the perpendicular electric field near the edges. It is found that near the edges

$$E_\perp \sim E_{\perp m} \sim E_o \quad . \tag{4}$$

We note that E_o depends on n_o and T_o; when n_o varies from 1 to 10 cm^{-3} and T_o from 1 to 100 eV, E_o ranges from about 100 to 1300 mV/m. Thus, the large perpendicular electric fields occurring near the edges of the current sheets resemble the phenomenon of electrostatic shocks observed in the auroral plasma Mozer et al. (1980).

Whether or not the double layers are well separated from the large $E_\perp$ near the current sheet edges, it is found that

$$E_{\parallel DL} << E_o \quad . \tag{5}$$

Depending on n_o and T_o, $E_{\parallel DL}$ may range from a few mV/m to several tens of mV/m. So far only weak double layers ($E_\parallel < 15$ mV/m) have been observed in space plasmas (Temerin et al., 1982).

We find that in the case of wide sheets it is possible to develop relatively large downward parallel electric fields outside the current sheets (panel a, Fig. 11). These fields drive downward return currents (panel c).

In these simulations we have seen both parallel and perpendicular accelerations of ions (Singh et al., 1986). Most energetic ions are seen to be at pitch angles near 90°. Ion beams are seen only in narrow sheets with thicknesses $\ell \lesssim \rho_H$.

It is found that the double layers play a key role in electron acceleration, even though, all the features of the accelerated electrons cannot be explained by a simple picture of electron acceleration by dc double layers. The double layers act as a trigger mechanism for a host of plasma processes, which determines the velocity distribution function of the accelerated electrons.

VII. PLASMA EXPANSION

Plasma expansions have been studied since the pioneering work of Gurevich et al. (1966), who studied the expansion of a plasma into a vacuum using the quasi-neutrality approximation. In this case the plasma equations allow self-similar solutions. However, this approximation breaks down in the low-density region where the local plasma Debye length becomes comparable to the scale length in the density gradient. Thus, a positive-negative charge separation occurs like in a double layer (Singh and Schunk, 1984b). However, it is worth noting that there is no current through such a double layer. The charge separation is supported by a relative smooth variation in the electron density while the ion density has a sharp density jump creating an ion density front. The plasma expansion is preceded by such a density front, behind which the self-similar solutions are found to be valid.

When a high-density (n_I) plasma expands into a plasma of low density (n_{II}), the expansion properties critically depend on the density ratio $R = n_I/n_{II}$ (Mason, 1971). An example of such a dependence is shown in Figure 12, in which we have compared the potential profiles associated with expanding plasmas as the ratio R is varied from R = 0.001 to 0.2. The potential profiles shown in this figure are obtained as follows. We consider that initially (time t = 0) the high- and low-density plasmas occupy the regions I ($x \leqslant 300\ \lambda_{di}$) and II, respectively. At times $t > 0$, the expansion is studied solving Vlasov equations for the ions in a self-consistent electric field obtained by solving the Poisson equation. The electrons are assumed to obey the Boltzmann law. In the calculations presented here we assume that the electron temperature $T_e = 10\ T_i$, where T_i is the initial ion temperature in regions I and II. The potential profiles shown in Figure 12 are at $t = 60\ \omega_{pi}^{-1}$, where ω_{pi} is the ion-plasma frequency in region I and $\lambda_{di} = V_{ti}/\omega_{pi}$ with V_{ti} being the ion thermal velocity. The different curves shown in Figure 12 are for different values of R as marked.

The noteworthy feature of the potential profile shown in Figure 12 is that as the density in region II is increased, the potential profiles steepen over a localized region in the expansion zone. When R is increased from 0.001 to 0.01, we note the formation of a "knee" in the potential profile near $x \sim 625\ \lambda_{di}$. When R is increased further this "knee" steepens and for n = 0.1 and 0.2 we note the presence of two sharp transitions in the potential profiles; one occurs in region I in which the rarefaction wave propagates in the backward direction, and the other occurs in the expansion region II. Near the transitions localized electric fields, like that in a double layer, occur. It is important to note that the sharp transitions in the potential profiles (double layers) occurring in regions I and II move in opposite directions. With increasing time the potential profile in region I becomes less and less steep while that near the sharp transition in region II maintains its profile giving a localized electric field nearly constant with time. The features associated with occurrence of localized electric fields also occur when a multi-ion plasma expands into a vacuum (Singh and Schunk, 1983b).

VIII. CONCLUSION

We have presented a brief summary of our studies related to the generation of electric fields in plasmas. Some of the mechanisms we discussed are as follows. When a potential drop is applied across a plasma, localized electric fields in the form of double layers occur. Double layers also form when a current is drawn through a plasma. The dynamical feature of such a double layer shows a cyclic behavior with a frequency determined by the transit time of the ions across an effective length of the system, in which the double layer forms. The formation of a potential dip at the low potential end of a DL and the current interruption are intimately related phenomena.

We have also discussed the generation of electric fields perpendicular to the ambient magnetic field in a plasma. Such fields can be generated by contact potentials near discontinuities in plasma properties. It was found that ion gyration plays an important role in generating the fields. The cases presented indicate that the scale length of the perpendicular electric field is of the order of the ion Larmor radius. Two complementary situations, in which perpendicular electric fields can be generated, were discussed. In one situation, we considered a low-density hot plasma sandwiched between high-density cold plasmas. It was shown that even if the hot ion density is low these ions are effective in creating electric fields of the magnitude observed in the auroral plasma. In the other situation, we considered a current sheet in a plasma. The density gradient across the sheet created the perpendicular electric fields. The formation of double layers in the sheet were studied.

The generation of electric fields in expanding plasmas was briefly discussed. It was shown that when a high-density plasma expands into a low-density plasma, the nature of the spatial distribution of the electric field critically depends on the density ratio of the two plasmas. A currentless double layer forms near the expanding plasma front.

Acknowledgment. This research was supported by NASA grant NAGW-77 and NSF grant ATM-8417880 to Utah State University.

REFERENCES

Alfvén, H., *Cosmic Plasma*, Reidel, Dordrecht, 1982.
Barakat, A. R., and R. W. Schunk, *J. Geophys. Res., 89,* 9771 (1984).
Block, L. P., *Cosmic Electrodyn., 3,* 349 (1972).
Borovsky, J. E., and G. Joyce, *J. Geophys. Res., 88,* 3116 (1983).
Carlqvist, P., *Cosmic Electrodyn., 3,* 377 (1972).
Coakley, P., and N. Hershkowitz, *Phys. Fluids, 22,* 1171 (1979).
Dubinin, E. M., et al., *Kosm. Issled, 23,* 466 (1985).
Evans, D. S., M. Roth, and S. Lemaire, "Electrical potential distribution at the inference between plasma sheet clouds," Presented at the Workshop on Double Layers in Astrophysics, Marshall Space Flight Center, Huntsville, Alabama, March 17-19, 1986.
Gurevich, A. V., L.–V. Pariiskaya, and L. P. Pitaevskii, *Sov. Phys. JETP, Eng. Transl., 22,* 449 (1966).
Hasegawa, A., and T. Sato, *Phys. Fluids, 25,* 632 (1982).
Hultqvist, B., *Planet. Space. Sci., 19,* 749 (1971).
Iizuka, S., P. Michelsen, J. J. Rasmussen, R. Schrittwieser, R. Hatakeyama, K. Saeki, and N. Sato, *Riso Report-M-2414,* Riso National Laboratory, Denmark, 1983.
Iizuka, S., P. Michelsen, J. J. Rasmussen, R. Schrittwieser, R. Hatakeyama, K. Saeki, and N. Sato, *J. Phys. Soc. (Japan), 54,* 2516 (1985).
Johnson, L. E., *J. Plasma Phys., 23,* 433 (1980).
Joyce, G., and R. F. Hubbard, *J. Plasma Phys., 20,* 391 (1978).
Kan, J. R., and S.-I. Akasofu, *J. Geophys. Res., 84,* 507 (1979).
Leung, P., A. Y. Wang, and B. H. Quon, *Phys. Fluids, 23,* 952 (1980).
Mason, R. J., *Phys. Fluids, 14,* 1943 (1971).
Morse, R. L., in *Computational Physics,* edited by Alder, Fernbach, and Rotinberg, Vol. 9, p. 213, Academic Press, New York, 1970.
Mozer, F. S., C. D. Cattell, M. K. Hudson, R. L. Lysak, M. Temerin, and R. B. Torbert, *Space Sci. Rev., 27,* 155 (1980).
Mozer, F. S., and M. Temerin, in *High-Latitude Space Plasma Physics,* edited by B. Hultqvist and T. Hagfers, p. 43, Plenum, New York, 1983.

Sato, T., and H. Okuda, *J. Geophys. Res., 86,* 3357 (1981).
Sestero, A., *Phys. Fluids, 7,* 44 (1964).
Silevitch, M. B., *J. Geophys. Res., 86,* 3573 (1981).
Singh, N., *Plasma Phys., 22,* 1 (1980).
Singh, N., *Plasma Phys., 24,* 639 (1982).
Singh, N., and R. W. Schunk, *J. Geophys. Res., 87,* 3561 (1982a).
Singh, N., and R. W. Schunk, *Geophys. Res. Lett., 9,* 1345 (1982b).
Singh, N., and R. W. Schunk, *Geophys. Res. Lett., 9,* 446 (1982c).
Singh, N., and R. W. Schunk, *J. Geophys. Res., 88,* 10081 (1983a).
Singh, N., and R. W. Schunk, *Phys. Fluids, 26,* 1123 (1983b).
Singh, N., and R. W. Schunk, *Plasma Phys. Controlled Fus., 26,* 859 (1984a).
Singh, N., and R. W. Schunk, in *Second Symposium on Plasma Double Layers and Related Topics,* edited by R. Schrittwieser and G. Eder, p. 272, University of Innsbruck, 1984b.
Singh, N., and H. Thiemann, *Geophys. Res. Lett., 8,* 737 (1980a).
Singh, N., and H. Thiemann, *Phys. Rev. Lett., 76A,* 383 (1980b).
Singh, N., H. Thiemann, and R. W. Schunk, *Geophys. Res. Lett., 10,* 745 (1983).
Singh, N., R. W. Schunk, and H. Thiemann, *Adv. Space Res., 4,* 481-490 (1984).
Singh, N., H. Thiemann, and R. W. Schunk, *J. Geophys. Res., 90,* 5173 (1985).
Singh, N., H. Thiemann, and R. W. Schunk, in *Ion Acceleration in the Magnetosphere and Ionosphere, Geophysical Monograph, 38,* edited by Tom Chang, pp. 343-347, AGU, Washington, D.C., 1986.
Temerin, M., K. Cerny, W. Lotko, and F. S. Mozer, *Phys. Rev. Lett., 48,* 1175 (1982).
Thiemann, H., N. Singh, and R. W. Schunk, *Adv. Space Res., 4,* 511 (1984).
Wagner, J. S., T. Tajima, J. R. Kan, J. N. Leboeuf, and J. M. Dawson, *Phys. Rev. Lett., 45,* 803 (1980).
Whipple, E. C., J. R. Hill, and J. D. Nichols, *J. Geophys. Res., 89,* 1508 (1984).

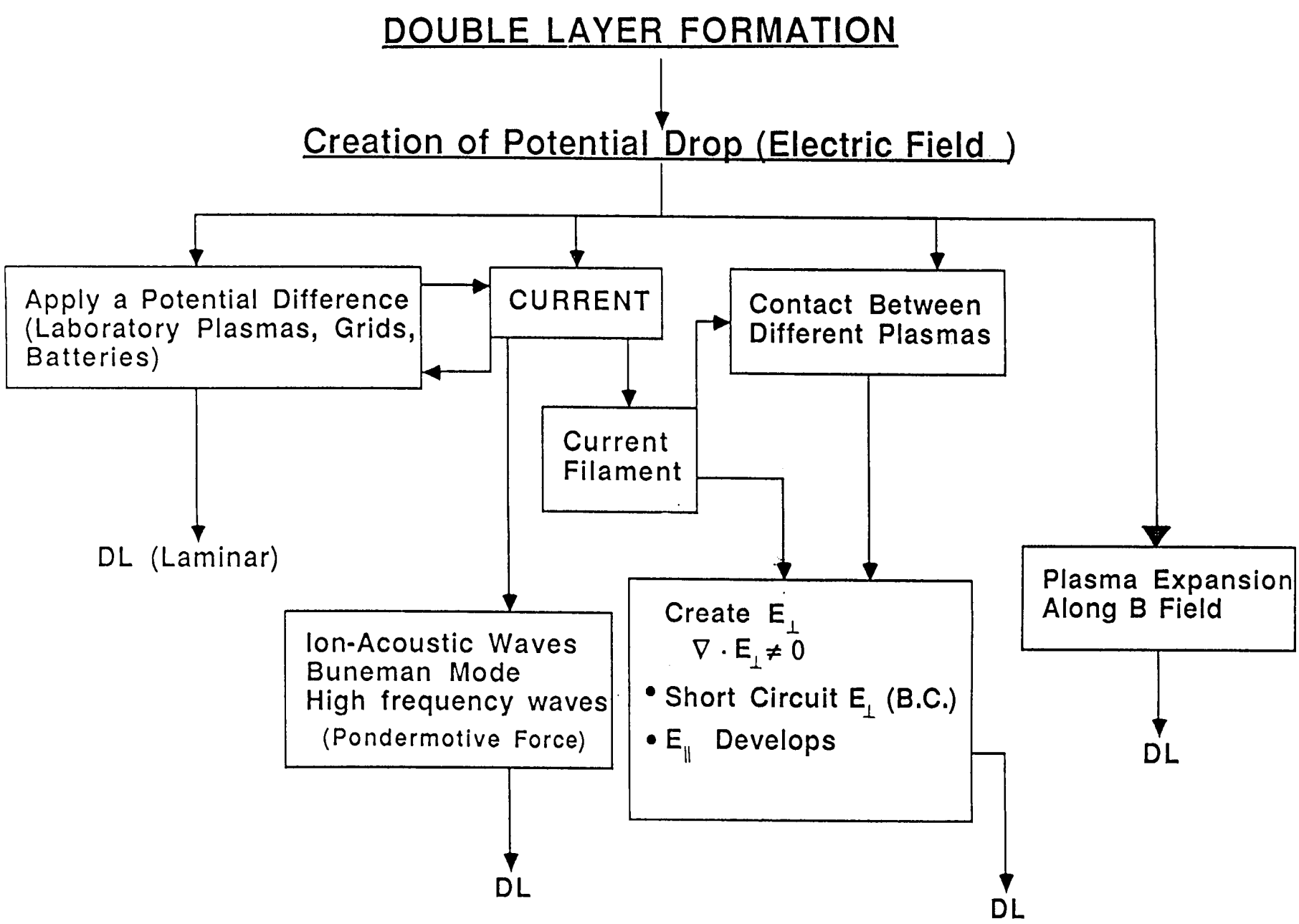

Figure 1. Summary of mechanisms for driving double layers.

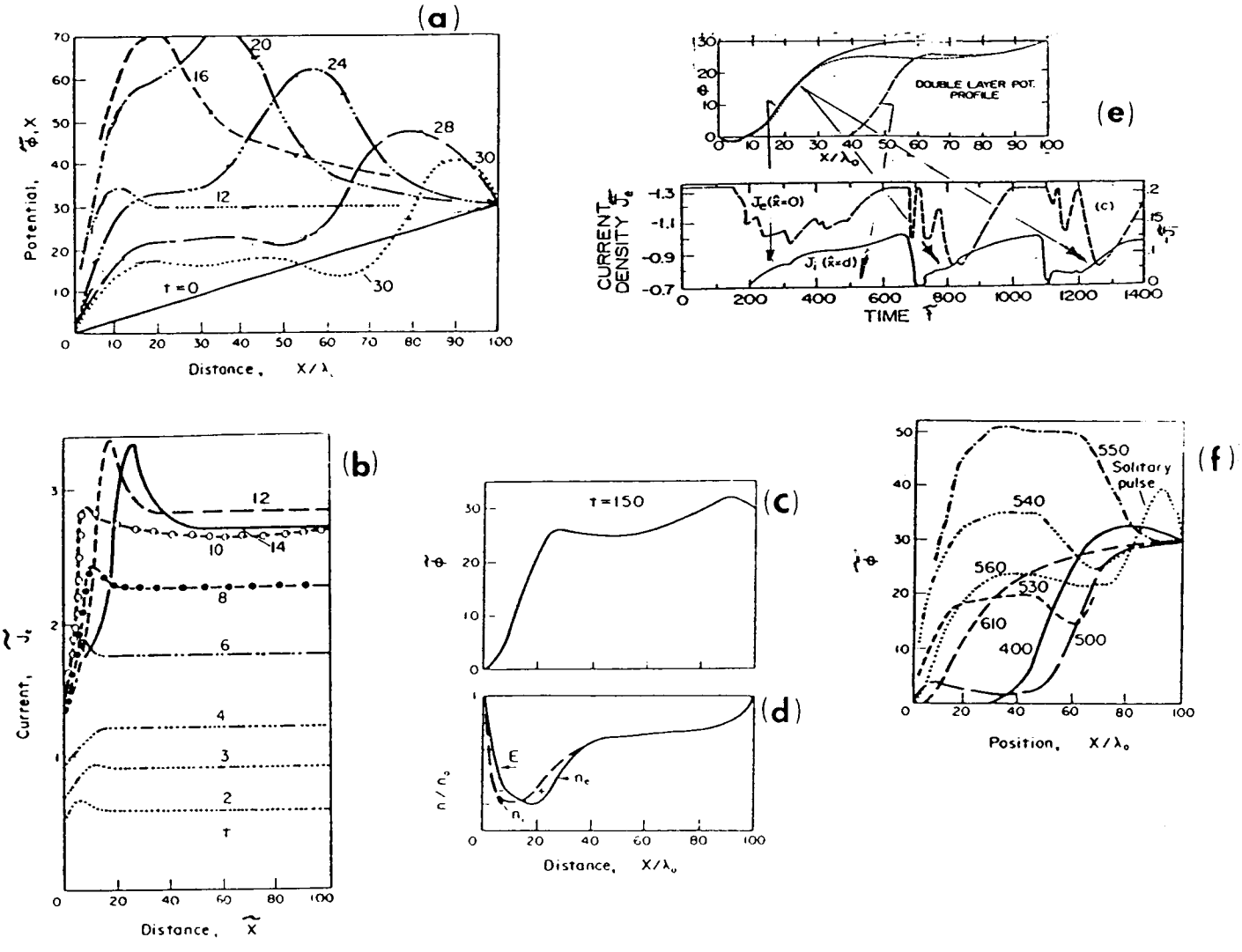

Figure 2. Double layer formation and dynamics as seen in one-dimensional Vlasov simulations. In the simulation, the plasma occupied the region $0 \leq x \leq 100\ \lambda_o$, where λ_o is the Debye length in the initial plasma ($t = 0$) across which a potential drop of $\Delta\phi_o = 30(k_B T_o/e)$ was applied, where T_o is the initial plasma temperature. We used the following normalizations: $\tilde{x} = x/\lambda_o$, velocity $\tilde{V} = V/V_{to}$, time $\hat{t} = t\omega_{po}$, temperature $\hat{T} = T/T_o$, potential $\tilde{\phi} = e\phi/k_B T_o$, current $\hat{J} = J/n_o e V_{to}$, where $V_{to} = (k_B T_o/m_e)^{1/2}$, ω_{po} is the electron plasma frequency with the initial density n_o, k_B is the Boltzmann constant, m_e is the electron mass, and $m_i/m_e = 64$, with m_i the ion mass; (a) temporal evolution of the potential profile, (b) temporal evolution of the current density profile, $\tilde{J}_e(\tilde{x})$, (c) double layer potential profile at $\tilde{t} = 150$, (d) density profiles and space charges supporting the DL in (c), and (e) recurring DL formation (top) and electron and ion current interruptions and recovery (bottom). The arrows indicate the times of the potential profiles; the arrows originating from the potential profiles marked with "A" indicate that these profiles correspond to the early stages of the electron current interruptions and to the beginning of the ion influx into the double layer during the three cycles of the double layer formation. Note the dip at the low potential end. The potential profile marked with "B" corresponds to the current recovery stage during the first cycle. (f) Potential profiles during a reformation of the DL; at $\tilde{t} = 400$ there is a DL, a positive potential perturbation near $x = 0$ is seen at $\tilde{t} = 500$; at later times this perturbation grows and eventually a new DL forms at $\tilde{t} \sim 610$.

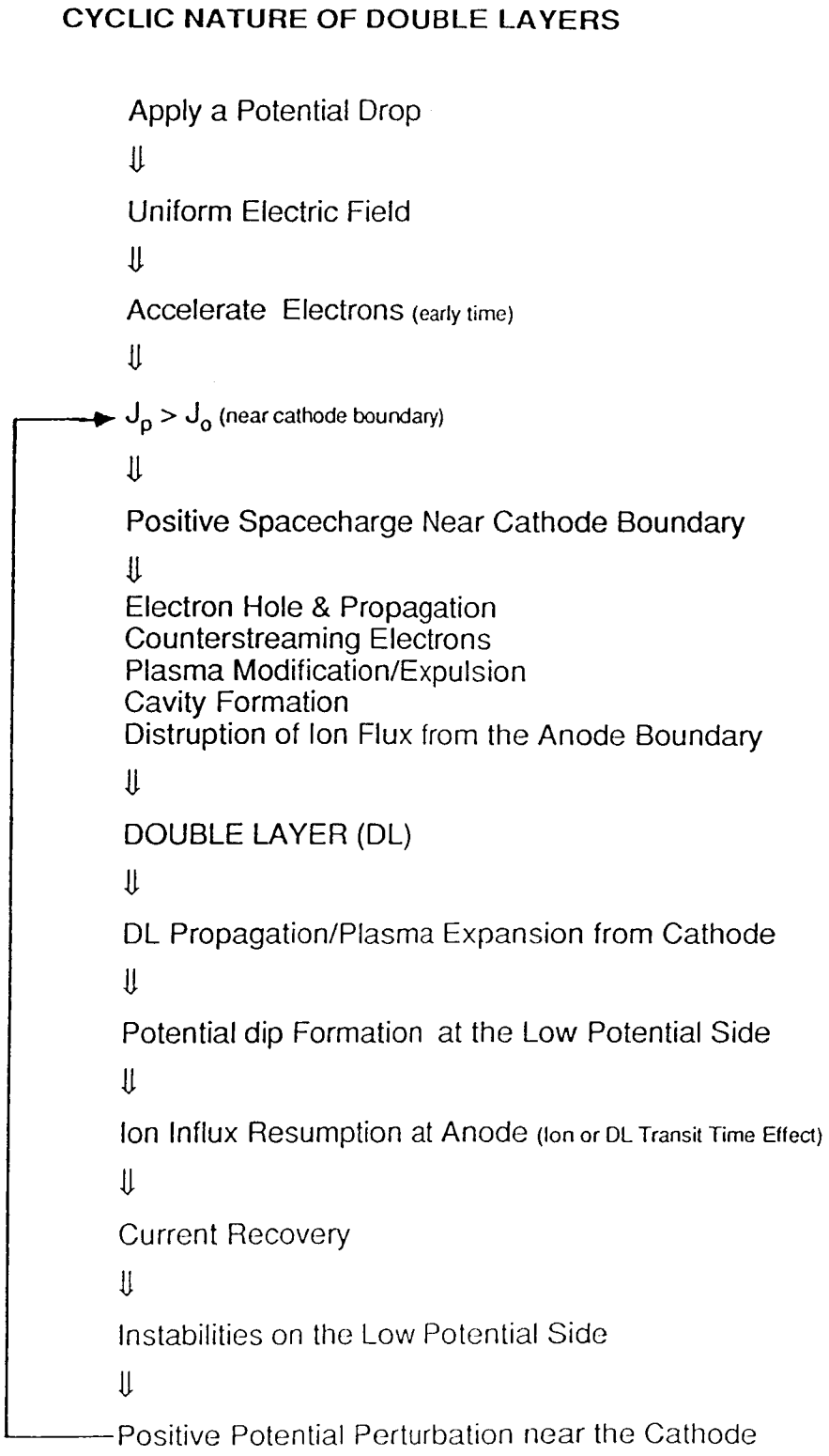

Figure 3. Summary of the various plasma processes occurring during the formation and reformation of a DL when a potential drop is applied across a plasma.

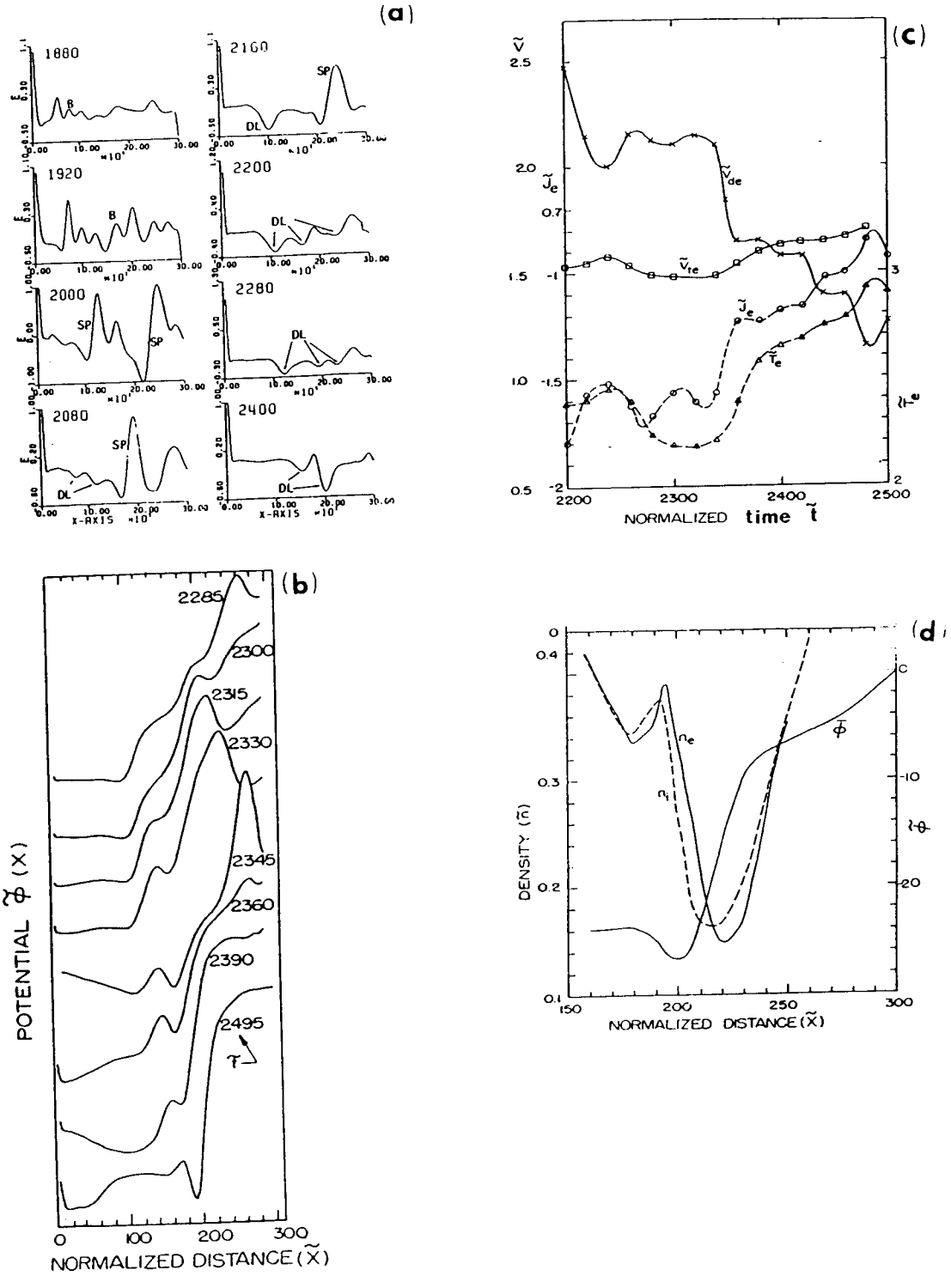

Figure 4. (a) Double layer evolution from the Buneman instability. Spatial profiles of the electric field E are shown at different times. At early times, $1880 < \tilde{t} < 2000$, small wavelength waves grow. At later times, in the nonlinear regime, these waves coalesce into long wavelength oscillations, which evolve into solitary pulses and double layers. (b) Temporal evolution of the double layer potential profile, (c) the corresponding temporal evolutions of the electron current J_e, electron drift velocity V_{de}, thermal velocity V_{te}, and temperature T_e at $\tilde{x} = 50$, and (d) spatial profiles of the electron and ion densities and the potential profile for a DL with a dip at its low potential end. The charge separation indicates the presence of a triple charge layer.

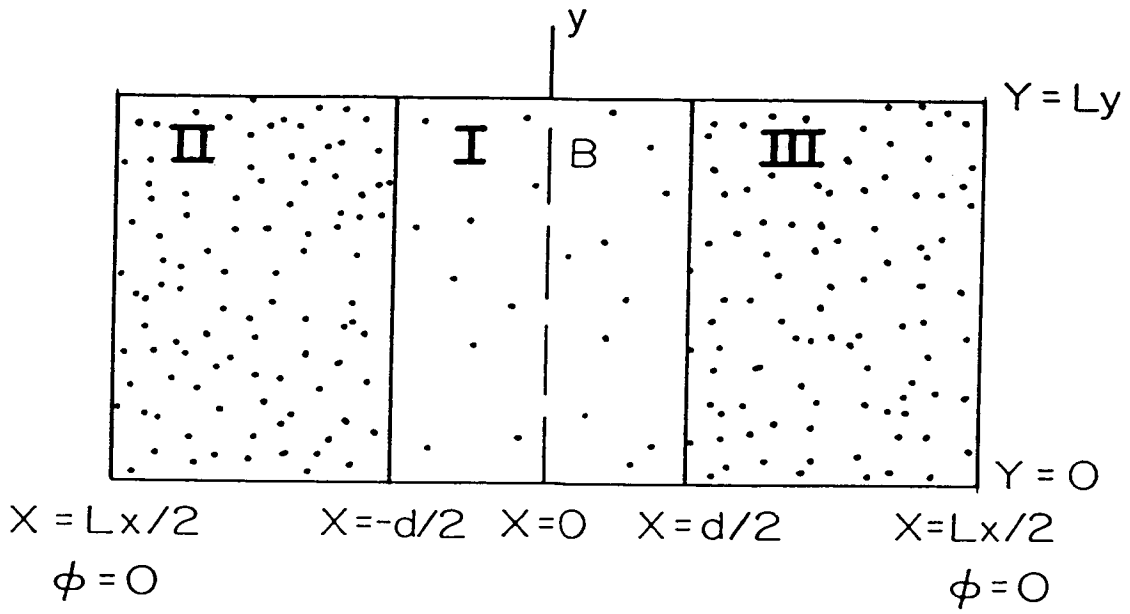

Figure 5. Geometry of the simulation scheme. A two-dimensional plasma of size $L_x \times L_y$ is simulated. Initially (t = 0), regions I to III are filled with plasmas. In the simulations described in this paper, the plasma in region I ($-d/2 < x < d/2$) is assumed to be hot, while the plasmas in regions II and III ($|x| > d/2$) are assumed to be cold and have similar properties. The **B** field is along the y-axis. The particles leaving the simulation plasmas at y = 0 and L_y are recirculated according to a periodic boundary condition, while those leaving at $x = \pm L_x/2$ are replaced from plasma reservoirs at the boundaries.

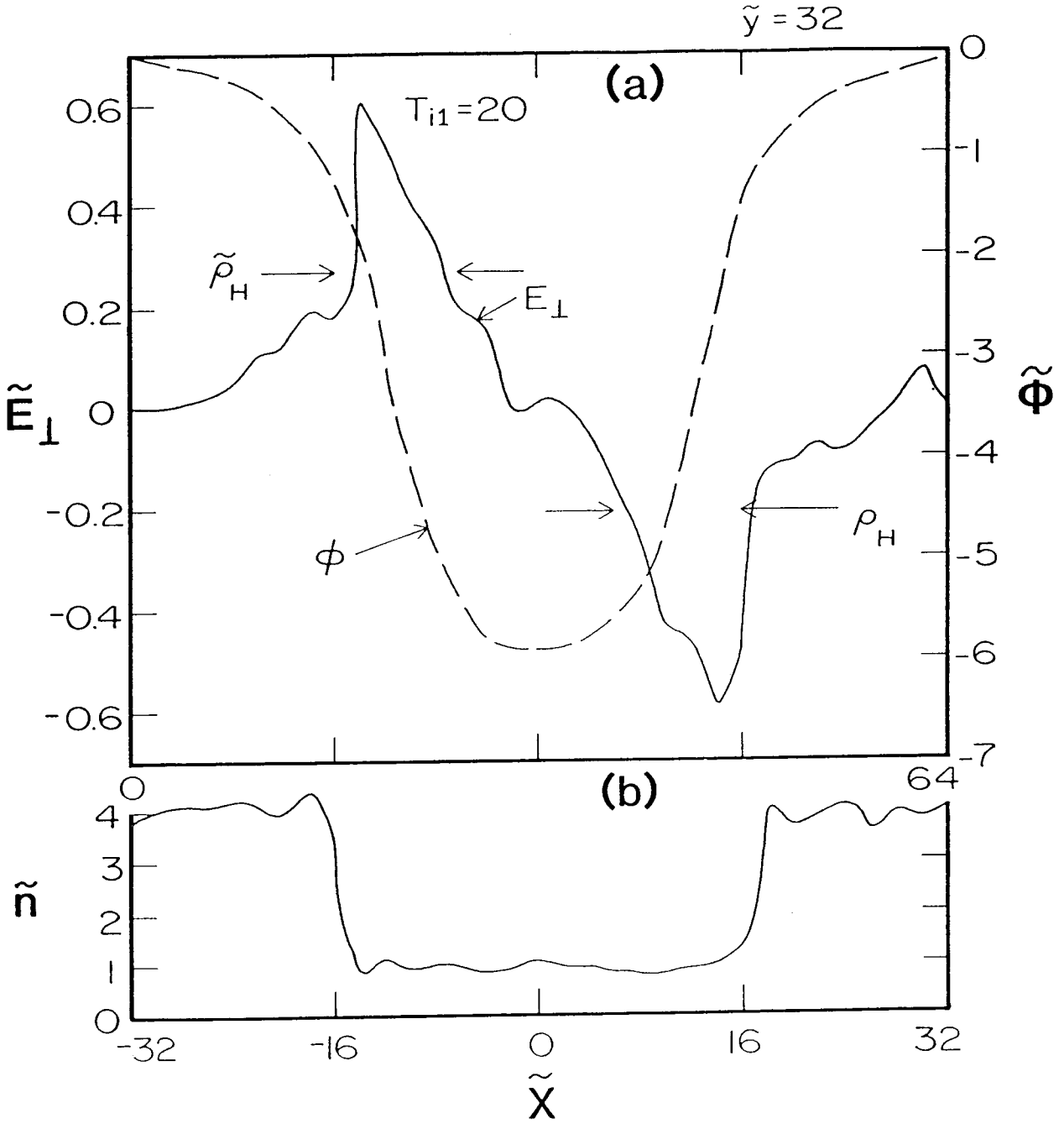

Figure 6. Variations of (a) electric potential and perpendicular electric field, and (b) plasma density as a function of x from a simulation with $\tilde{T}_{i1} = 20$. The average value of the hot in Larmor radius ρ_H is indicated in (a).

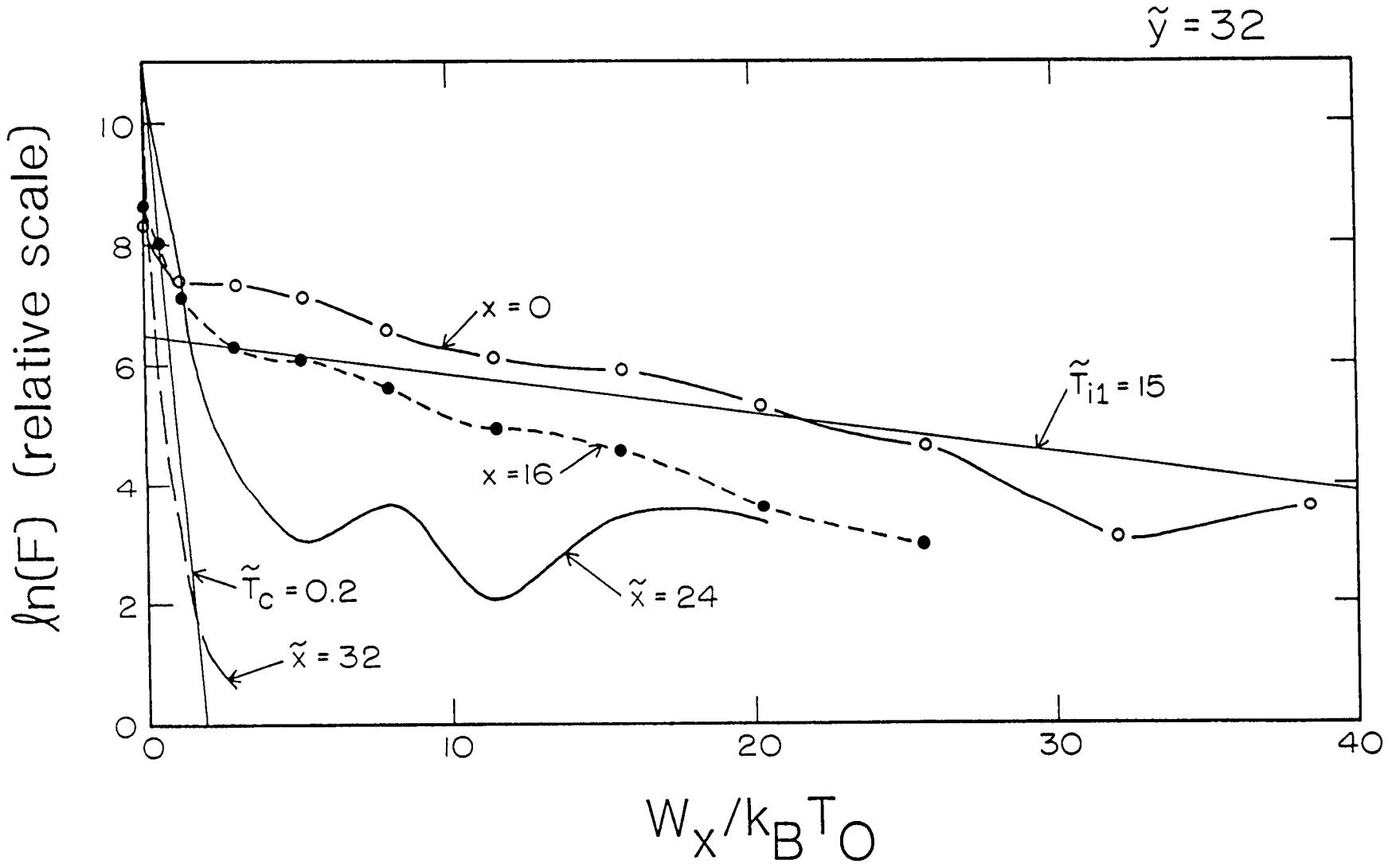

Figure 7. Ion energy distribution function $F(W_x = 1/2\ m_i V_x^2)$ at several locations for $x \geq 0$. The distribution functions for $x < 0$ are nearly the same. Note that the two asymptotes marked with $\tilde{T}_{i1} = 15$ and $\tilde{T}_c \simeq 0.2$ show the initial Maxwellian distributions.

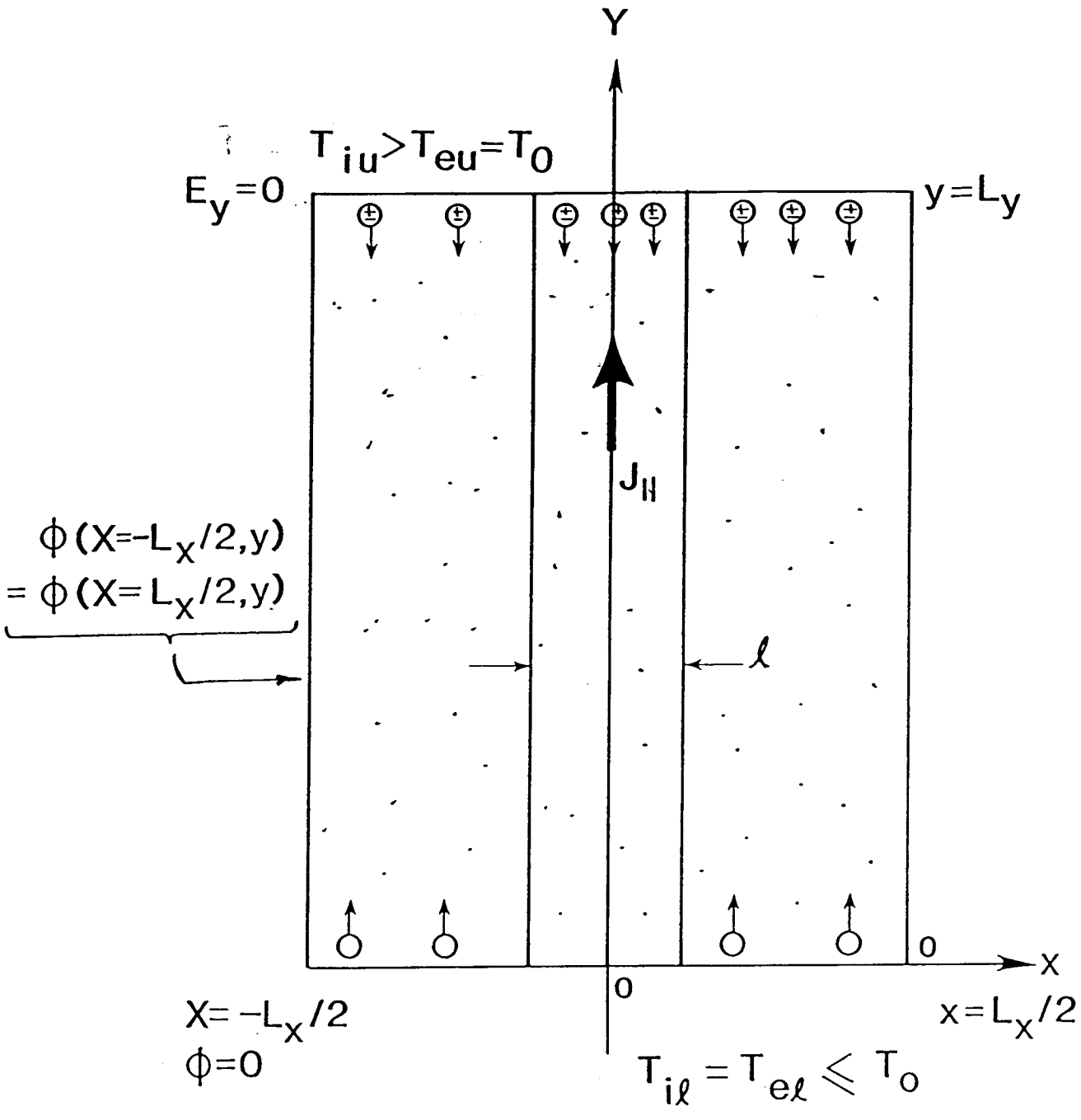

Figure 8. Scheme for simulating double layers driven by a current sheet.

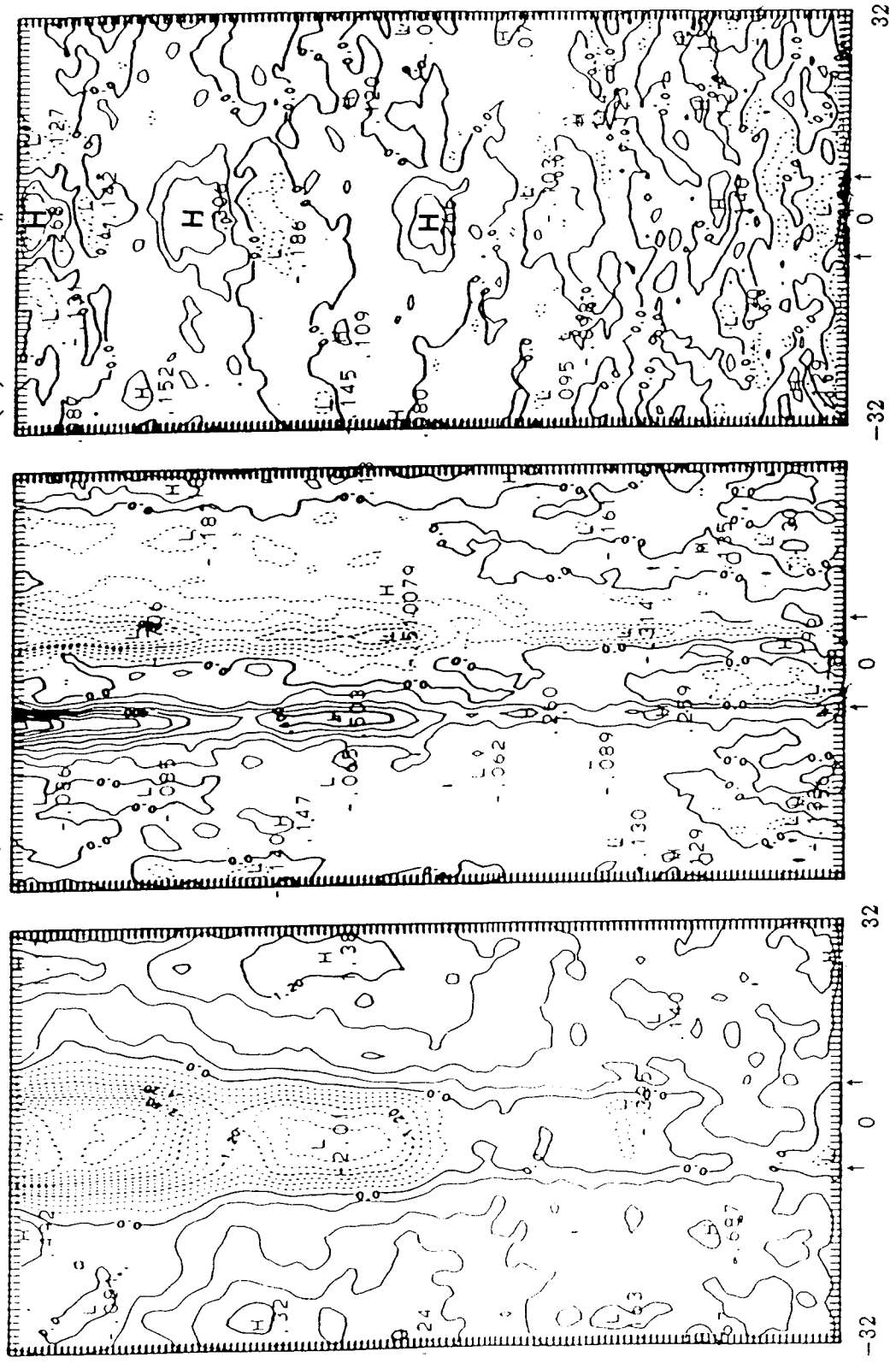

Figure 9. Potential structure driven by a current sheet with $\ell = 12\,\lambda_{do}$, $\rho_H = 9\,\lambda_{do}$, $J_o = 1.25\,en_oV_{to}$; (a) equipotential surfaces, (b) contours of constant $E_\perp$, and (c) contours of cosntant $E_\parallel$. The contour intervals are indicated on the top of the panels. The edges of the sheet are indicated by the arrows at the bottom of the panels.

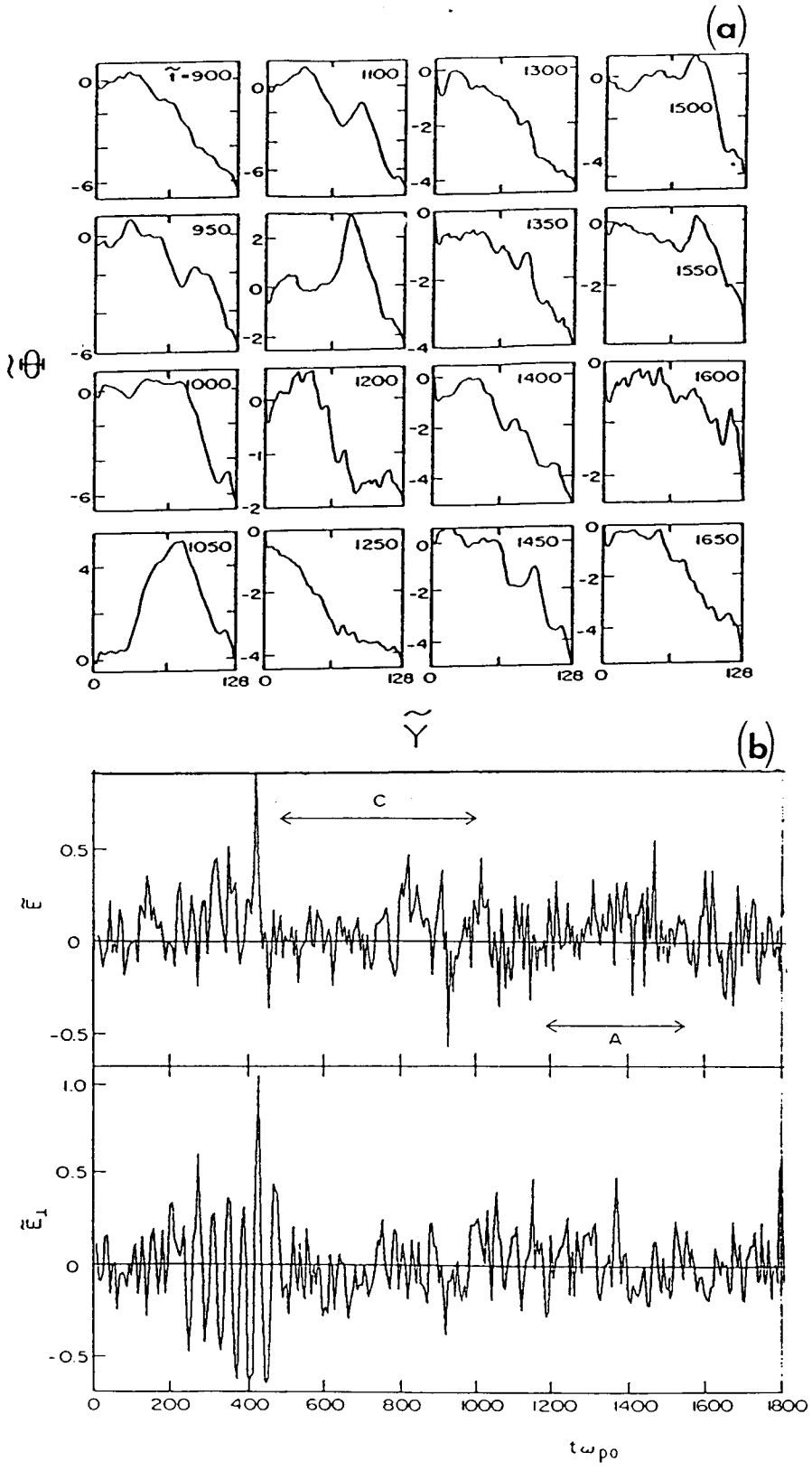

Figure 10. (a) Temporal evolution of the double layer potential profile along the axis of the current shown in Figure 8 and (b) fluctuations in $E_\parallel$ and $E_\perp$ in the region of the DL formation.

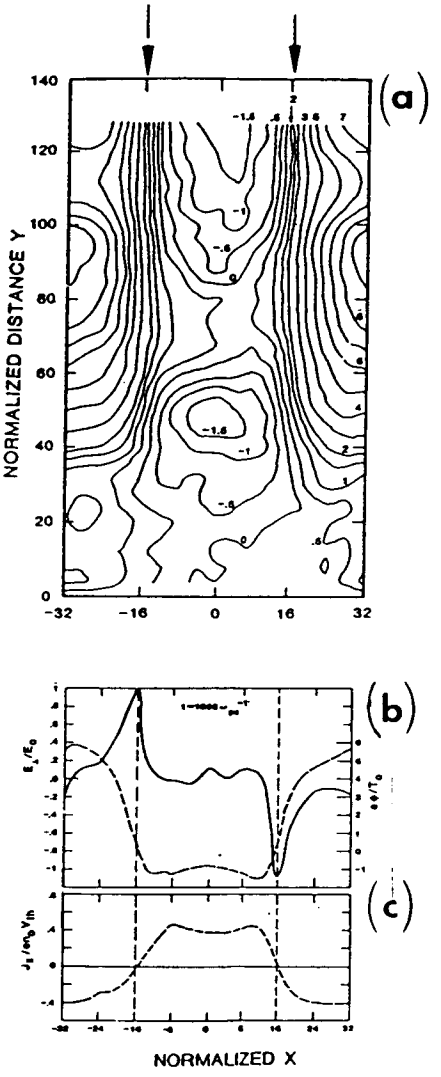

Figure 11. (a) Potential structure associated with a wide current sheet, with $\ell = 32\,\lambda_{do}$, $\rho_H = 3\,\lambda_{do}$, and $J_o = 0.6\ n_o e V_{to}$. The current sheet edges are indicated by the arrows at the top of the panel. Equipotential surfaces are shown. (b) Perpendicular distribution of $E_\perp$ and ϕ near the top ($\bar{y} = 1120$) of the potential structure in (a). Note that $E_\perp$ is primarily confined near the edges of the current sheet. (c) Perpendicular distribution of the parallel current density $J_\parallel$; note the positive (upward) current inside the sheet, while outside the sheet the current is negative (downward). The downward current is caused by the upward acceleration of the electrons by the downward (parallel) electric field (see the potential distribution outside the sheet in (a)).

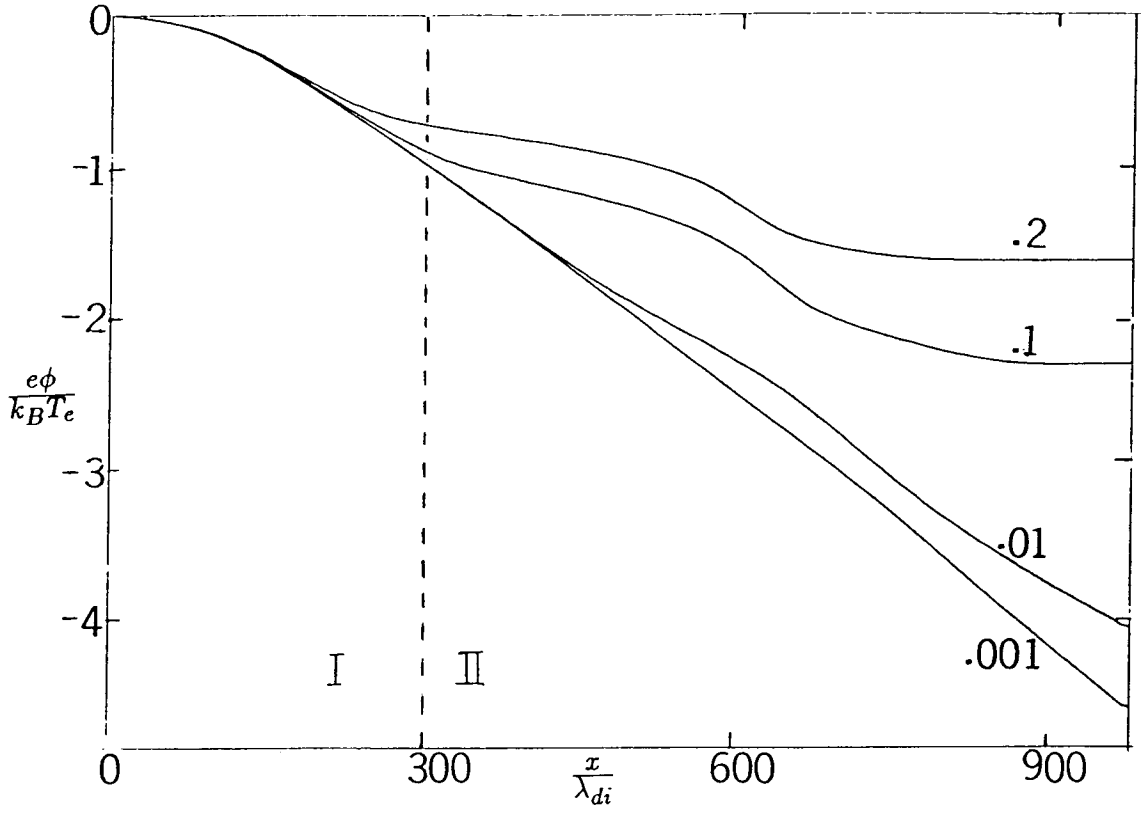

Figure 12. Snapshot ($t = 60\ \omega_{po}^{-1}$) of the potential profile associated with the expansion of a high-density plasma into region II. The different profiles are for different values of the density ratio n_I/n_{II}, as indicated.